$Mn^{2+} > Zn^{2+}$; (ii) the rate constants for the Mg^{2+} and Mn^{2+} enzymes have much higher values than can be explained in terms of known effects observed in the model reactions.[41] It appears that although the $oxac^{2-}$ is bound to the divalent metal ion in the enzyme, other enzyme functional groups assist in the CO_2-loss mechanism.

In contrast, Zn(II) is a poor activator of the catalytic mechanism. The low activity of Zn(II) pyruvate kinase is not unique to oxac decarboxylation since this form of the enzyme also shows low activity in the phosphoryl transfer function.[40] Zn(II) appears to be too strong a Lewis acid for the enzyme and possibly binds additional groups that need to be free to achieve maximum activity.

While it is not at this time possible to say with certainty in what way the enzyme might promote decarboxylation, a likely mode is through proton donation. It should be noted that a proton is required as pyruvate kinase catalyzes the transfer of a phosphoryl group from phosphoenol pyruvate. The same proton donor might also be involved in promoting oxac decarboxylation, and it is significant that enol pyruvate is formed in both reactions. A possible mechanism might involve interactions and reactions such as (7).

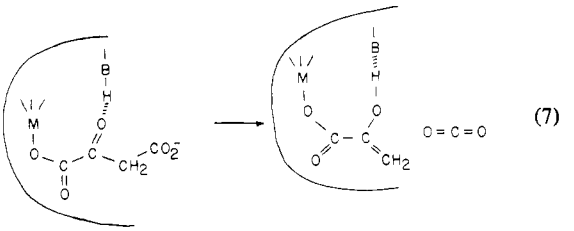

(7)

According to this picture the metal ion chelate of pyruvate enolate is replaced by one involving the metal ion and another enzyme group. The advantage gained by the enzyme is a favorable prereaction geometry and the formation of a strong O-H bond, which maintains the chelate structure.

Some evidence that proton donation can indeed assist metal ion catalyzed decarboxylation has been obtained in studies on the models in 50% dioxane. There the pathway Mg(oxac) + HOAc $\rightleftharpoons$ CO_2 + $Mg(pyu)^+$ + Oac^- was found.[17] These studies are being pursued to uncover more details of how coordinated oxac may be activated by other components of a reaction mixture.

Acknowledgment. We express our appreciation to the National Science Foundation for its generous support of this research. Helpful conversations with Dr. Perry Frey are also acknowledged.

Registry No. Oxalacetate, 328-42-7; Mg, 7439-95-4; Mn, 7439-96-5; Zn, 7440-66-6; PK, 9001-59-6.

(40) P. F. Solvonuk and H. B. Collier, *Can. J. Biochem. Physiol.*, **33**, 38 (1955).
(41) It has been suggested[5] that enzyme groups coordinated to the divalent metal ion can alter its electron density sufficiently to influence the decarboxylation rate. We have found[16,42] that such effects on the decarboxylation rates of mixed-ligand complexes containing $oxac^{2-}$ are either negligible or far too small to account for the enzymic rates observed here. While Rund and Claus[43] have reported that the presence of 1,10-phenanthroline markedly increases the rate by which α,α-dimethyloxalacetate is decarboxylated by Mn^{2+}, they also report no effects of this ligand on the rates of the Mg^{2+}-catalyzed reaction. Since our data show that the highest ratio of enzymatic rate to binary complex rate occurs with Mg^{2+}, the results of Rund and Claus lend further support to the view that activation of the metal ion by the enzyme is not an important feature of this reaction. We have also found[44] that the Mn-phen system reverts to normal behavior when air is rigorously excluded.
(42) Ralph K. Steinhaus, N. V. Raghavan, and D. L. Leussing, *J. Inorg. Nucl. Chem.*, **39**, 1871 (1977).
(43) John V. Rund and Kenneth G. Claus, *J. Am. Chem. Soc.*, **89**, 2256 (1967).
(44) B. J. Lillis, to be reported.
(45) T. L. James and M. Cohn, *J. Biol. Chem.*, **249**, 3519 (1974).

Contribution from the Institut für anorganische und physikalische Chemie, Universität Bern, CH-3000 Bern 9, Switzerland, the Institut für Reaktortechnik, Eidgenössische Technische Hochschule Zürich, CH-5303 Würenlingen, Switzerland, and the Risø National Laboratory, DK-4000 Roskilde, Denmark

Intra- and Intermolecular Interactions in $[Ni_2(ND_2C_2H_4ND_2)_4Br_2]Br_2$. A Study by Inelastic Neutron Scattering and Magnetic Measurements

ANTON STEBLER,[1a] HANS U. GÜDEL,*[1a] ALBERT FURRER,[1b] and JØRGEN K. KJEMS[1c]

Received February 13, 1981

$[Ni_2(ND_2C_2H_4ND_2)_4Br_2]Br_2$ was studied by inelastic neutron scattering (INS) and magnetic measurements. Intramolecular energy splitting due to exchange interactions and magnetic anisotropy were directly determined by INS. The exchange coupling is ferromagnetic with $J = 3.55 \pm 0.20$ cm^{-1}; the anisotropy is axial with $D = -6.8 \pm 0.8$ cm^{-1} and $E = 0 \pm 0.8$ cm^{-1}. Information on the intermolecular coupling was obtained from the low-temperature magnetization. The coupling is antiferromagnetic with $J' = -0.25 \pm 0.05$ cm^{-1}.

1. Introduction

Complexes of the type $[Ni_2(en)_4X_2]^{2+}$, where X = Cl^-, Br^-, or SCN^- (Figure 1), are well-known dimers with ferromagnetic intramolecular coupling.[2a] The ferromagnetic nature of the exchange coupling was deduced from the magnetic susceptibility. A number of linear chain compounds with very similar $Ni(\mu\text{-}X)_2Ni$ bridging geometries also exhibit ferromagnetic behavior.[2b] The principal difficulty in properly describing the electronic ground-state properties of a compound like $[Ni_2(en)_4Br_2]Br_2$ arises from the single-ion anisotropy energies having the same order of magnitude, that is, a few wavenumbers, as the exchange interaction energies. The two effects compete, and as a result, the energy splitting pattern may not be simple. Furthermore, even though the shortest intermolecular Ni-Ni distance is 7.8 Å in the bromide,[3] interdimer interactions cannot a priori be excluded due to the ferromagnetic intradimer interaction. They are usually incorporated in the effective Hamiltonian by a molecular field term.[2a] In the least-squares procedures used to extract parameters from the magnetic susceptibility data, the molecular field parameter J' is highly correlated with the intramolecular parameters J

(1) (a) Universität Bern. (b) Technische Hochschule Zürich. (c) Risø National Laboratory.
(2) (a) Ginsberg, A. P.; Martin, R. L.; Brookes, R. W.; Sherwood, R. C. *Inorg. Chem.* **1972**, *11*, 2884. (b) Witteveen, H. T.; Rutten, W. L. C.; Reedijk, J. *J. Inorg. Nucl. Chem.* **1975**, *37*, 913.
(3) Antsyshkina, A. S.; Porai-Koshits, M. A. *Dokl. Akad. Nauk SSSR* **1962**, *143*, 105.

0020-1669/82/1321-0380$01.25/0

Table I. Literature Results of Magnetochemical Studies of $[Ni_2(en)_4Cl_2]Cl_2$[a]

J	D	E	J'	Θ	g	expt	ref
9.9 ± 2.9	−6.5 ± 5.8		−0.17 ± 0.05		2.14 ± 0.03	powder susceptibility	2a
10.4 ± 2.4	11.1 ± 2.0		−0.02 ± 0.04		2.12 ± 0.03	same data set	2a
2.55	−10.0	2.0				powder susceptibility	6
6.65 ± 0.1	−3.6 ± 0.1			2.1 ± 0.4	2.211 ± 0.003	same data set	4
6.7 ± 0.1	−0.5 ± 0.5			2.1 ± 0.4	2.211 ± 0.003	same data set	4
3.5 ± 0.4	−9.7 ± 0.7		−0.21 ± 0.07		2.25 ± 0.02	single-crystal susceptibility	5

[a] The parameters are adapted to the conventions used in this work. Θ is a Weiss constant. Energy values are in cm^{-1}.

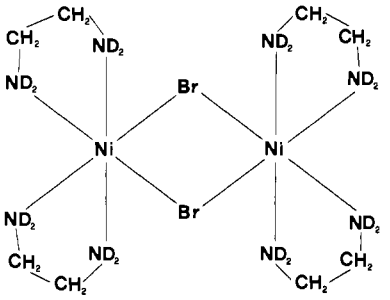

Figure 1. Schematic representation of the complex.

(exchange interaction) and D and E (anisotropy).

It is therefore very difficult to extract a unique set of parameters and to separate intra- and intermolecular effects. Attempts have been made to solve this problem by investigating a series of related compounds,[4] by measuring anisotropic magnetic susceptibilities on single crystals,[5] and by measuring complementary heat capacities.[6]

Spectroscopic methods, in particular those that do not require an external magnetic field, can be of high value. Ideally they allow the measurement of the molecular properties, which are only very weakly perturbed by small intermolecular interactions. Unfortunately there are a number of difficulties in the direct measurement of low-lying electronic states (on the order of 1–1000 cm^{-1}) with most of the relevant spectroscopic methods.

The energy splittings are too large for direct determination by EPR, but the method can provide valuable information on the nature of the low-lying states and the splittings may be estimated from the temperature dependence. Far-infrared and Raman spectroscopy, which cover the spectral range of interest, suffer in their applicability from the selection rule $\Delta S = 0$. Optical spectroscopy has been widely used to determine exchange splittings in chromium(III) systems.[7,8] The small line width of the $^4A_2 \rightleftarrows {}^2E$ transitions enables the direct determination of ground- and excited-state splittings. Except for chromium(III), which is exceptionally favorable in that respect, optical spectroscopy has not found wider application in this field.

Inelastic neutron scattering (INS) has been used for a long time to study crystal field and cooperative-exchange effects in rare-earth and transition-metal compounds. Its application to the study of exchange-coupled clusters of paramagnetic transition-metal ions is quite recent.[9] Splittings of the order of a few to a few hundred wavenumbers are accessible by INS. Since spin as well as orbital angular momentum can interact with the neutrons in the scattering process, contrary to the purely orbital mechanism in IR and Raman spectroscopy, transitions with $\Delta S = \pm 1$ are allowed. Exchange splittings in pure spin systems can therefore be measured. In the present study of $[Ni_2(en)_4Br_2]Br_2$ we are trying to combine magnetic and spectroscopic methods to obtain a description of both molecular properties and intermolecular interactions. The need for such an investigation is illustrated in Table I, which summarizes the conclusions of various magnetochemical studies on the related system $[Ni_2(en)_4Cl_2]Cl_2$. The bromide rather than the chloride was chosen in our work for practical experimental reasons. Chlorine atoms have a rather large incoherent nuclear scattering contribution, which adds an unwanted background to the INS experiments. For the same reason the N-deuterated compound was investigated. In the remainder of the paper, unless otherwise stated, en is used as an abbreviation of $ND_2CH_2CH_2ND_2$.

2. Experimental Section

2.1. Synthesis and Crystal Growth. A literature procedure was used for the preparation of undeuterated $[Ni_2(en)_4Br_2]Br_2$.[10] For the synthesis of $[Ni_2(ND_2C_2H_4ND_2)_4Br_2]Br_2$ the procedure was adapted with H_2O and CH_3OH replaced by D_2O and CH_3OD respectively. After four recrystallizations from D_2O/CH_3OD a product was obtained, which had a degree of deuteration at the nitrogen atoms of 91 ± 1%. Single crystals of up to 25 × 7 × 7 mm^3 were obtained by slow diffusion of ether into a D_2O/CH_3OD solution of the complex.

2.2. Inelastic Neutron Scattering. The N-deuterated product was used for all the measurements. For the powder measurements the sample was sealed in a cylindrical aluminum container (diameter 1 cm, length 5 cm). For the single-crystal experiments four of the largest crystals were mounted with their crystallographic axes parallel to within 2°. Measurements were made both at the Saphir reactor at Würenlingen, Switzerland, and at the DR3 reactor at Risø National Laboratory in Denmark. A multiangle reflecting crystal (MARC) spectrometer was used at Würlingen, and a triple-axis spectrometer (TAS 7) was used at Risø. A cold source was used at Risø, with a resulting gain in both intensity and resolution.

For the single-crystal experiments the crystals were mounted with their monoclinic b axes perpendicular to the scattering plane. With this orientation the projections of all the Ni–Ni vectors $\vec{R}$ on the scattering plane are parallel, and it is possible to make experiments for well-defined values of $\vec{R}\cdot\vec{Q}$, where $\vec{Q}$ is the scattering vector. The scalar product is important in the theoretical interpretation (vide infra). All the INS experiments were performed at temperatures below 15 K with a single exception. In the analogous chloride compound a structural transition had been found to occur around 20 K.

2.3. Magnetic Measurements. A moving-sample technique[11] was used for the magnetization and susceptibility measurements. All the measurements were made on freshly powdered samples. A diamagnetic correction of -349.4×10^{-6} cm^3 (mol of dimer)$^{-1}$ was applied to the magnetic data.

3. Theory

3.1. Inelastic Neutron Scattering. The pair functions are designated $|S_aS_bSM\rangle$ or simply $|SM\rangle$ since $S_a = S_b = 1$. The spin Hamiltonian can be written as

$$\hat{H}_{\text{eff}} = -2J(\hat{S}_a\cdot\hat{S}_b) + D\{[S_a^z]^2 + [S_b^z]^2 - \tfrac{4}{3}\} + E\{[S_a^x]^2 - [S_a^y]^2 + [S_b^x]^2 - [S_b^y]^2\} \quad (1a)$$

The functions $|S_aS_bSM\rangle$ are not eigenfunctions of (1a). Appropriate combinations have to be constructed, resulting

(4) Journaux, Y.; Kahn, O. *J. Chem. Soc., Dalton Trans.* **1979**, 1575.
(5) Joung, K. O.; O'Connor, C. J.; Sinn, E.; Carlin, R. L. *Inorg. Chem.* **1979**, *18*, 804.
(6) Journaux, Y.; Kahn, O.; Chevalier, B.; Etourneau, J.; Claude, R.; Dworkin, A. *Chem. Phys. Lett.* **1978**, *55*, 140.
(7) Ferguson, J.; Güdel, H. U. *Chem. Phys. Lett.* **1972**, *17*, 547.
(8) Ferguson, J.; Güdel, H. U.; Puza, M. *Aust. J. Chem.* **1973**, *26*, 513.
(9) Güdel, H. U.; Furrer, A. *Mol. Phys.* **1977**, *33*, 1335.
(10) State, H. M. *Inorg. Synth.* **1960**, *6*, 198.
(11) Rebouillat, J. P. Doctoral Dissertation, CNRS, Grenoble, 1972.

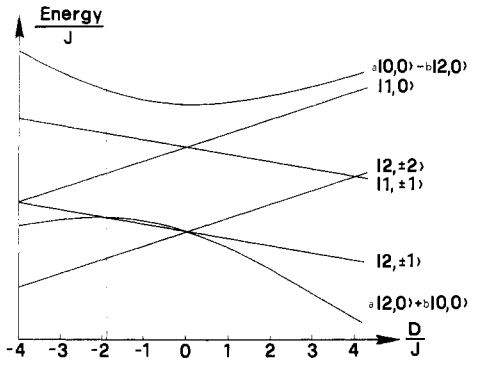

Figure 2. Energy splitting as a function of D/J for an axial magnetic anisotropy. The dashed line corresponds to the final result.

in a severe complication of the formalism for the INS cross section. Since it turned out (vide infra) that the observed splitting pattern can be well described by a spin Hamiltonian with axial anisotropy only, the operator shown in (1b) will be

$$\hat{H}_{\text{eff}} = -2J(\hat{S}_a \cdot \hat{S}_b) + D\{[S_a^z]^2 + [S_b^z]^2 - \tfrac{4}{3}\} \quad (1b)$$

used. With the exception of $|00\rangle$ and $|20\rangle$ the $|SM\rangle$ functions are eigenfunctions of (1b). Figure 2 shows an energy correlation diagram. INS allows the measurement of transitions between the various levels in Figure 2.

The differential cross section of a transition $|SM\rangle \rightarrow |S'M'\rangle$ is given by

$$\frac{d^2\sigma}{d\Omega\, d\omega} = \frac{N}{Z}\left(\frac{g\gamma r_0}{2}\right)^2 \frac{k_1}{k_0}(F^2(\vec{Q}))\exp(-2W) \times \exp\left(-\frac{E_{S,M}}{k_B T}\right)\sum_{\alpha,\beta}\left(\delta_{\alpha\beta} - \frac{Q_\alpha Q_\beta}{Q^2}\right)\sum_{ij}\exp[i\vec{Q}\cdot(\vec{R}_i - \vec{R}_j)]\langle SM|\hat{S}_i^\alpha|S'M'\rangle\langle S'M'|\hat{S}_j^\beta|SM\rangle\delta(\hbar\omega + E_{S,M} - E_{S',M'}) \quad (2)$$

The symbols in (2) have been explained before.[9] Of interest to us are: $F(\vec{Q})$, the magnetic form factor; $\vec{R}_i$, the position vector of the ith Ni ion in the molecule; $\vec{Q}$, the scattering vector; and the matrix element $\langle SM|\hat{S}_i^\alpha|S'M'\rangle$. α and β stand for x, y, and z.

Using tensor operator techniques for the evaluation of the matrix elements in (2), we find the selection rules

$$\Delta S = 0, \pm 1 \qquad \Delta M = 0, \pm 1 \quad (3)$$

The $\vec{Q}$ dependence of intensity of a transition $|SM\rangle \rightarrow |S'M'\rangle$ is shown to be

$$I(Q) \propto (F^2(\vec{Q}))[1 + (-1)^{S-S'}\cos(\vec{Q}\cdot\vec{R})] \times 2\sum_\alpha\left(1 - \frac{Q_\alpha^2}{Q^2}\right)|\langle SM|\hat{S}_a^\alpha|S'M'\rangle|^2 \quad (4)$$

The expression in square brackets in (4) is a so-called interference term.[12] The intensity critically depends on the relative orientation of $\vec{Q}$ and $\vec{R}$, where $\vec{R}$ is the vector connecting the two nickel(II) centers in the dimer. Transitions with $\Delta S = 0$ are expected to exhibit maximum intensity when $\vec{Q}$ and $\vec{R}$ are orthogonal and zero intensity when $\vec{Q}\cdot\vec{R} = \pi$. For $\Delta S = \pm 1$ transitions the situation is opposite, maximum for $\vec{Q}\cdot\vec{R} = \pi$ and zero for $\vec{Q}\cdot\vec{R} = 0$.

The term $(1 - Q_\alpha^2/Q^2)$ contains the dependence of the intensity on the axes defining the crystal field anisotropy. They are not known. The dimeric complexes are distorted, retaining a center of inversion as the only symmetry element.[3,5] As an approximation we can assume either C_3 or C_{2v} single-ion point symmetry. In the latter case the twofold axis coincides with the Ni–Ni direction, and the z axis of the crystal field anisotropy is perpendicular to the $Ni(\mu\text{-}Br)_2Ni$ plane. This was our choice of z for the intensity calculations. The result would not be strongly altered by choosing the approximate threefold axis as z. Our choice of z is compatible with the results of measurements of the magnetic susceptibility anisotropy of the related chloride compound.[5]

For the interpretation of a powder experiment, (4) has to be averaged in $\vec{Q}$ space. The resulting Q dependence for $|SM\rangle \rightarrow |S'M'\rangle$ transitions with $\Delta M = 0$ and $\Delta M = \pm 1$ are given in formulas 5 and 6, respectively. We thus have four different

$$\Delta M = 0: \quad I(Q) \propto (F^2(Q))\left\{\frac{2}{3} + (-1)^{S-S'}\left[\frac{2\sin QR}{Q^3R^3} - \frac{2\cos QR}{Q^2R^2}\right]\right\} \quad (5)$$

$$\Delta M = \pm 1: \quad I(Q) \propto (F^2(Q))\left\{\frac{2}{3} - (-1)^{S-S'}\left[\frac{\sin QR}{Q^3R^3} - \frac{\cos QR}{Q^2R^2} - \frac{\sin QR}{QR}\right]\right\} \quad (6)$$

Q dependencies for the four types of transition with $\Delta S = 0$, ± 1 and $\Delta M = 0$, ± 1.

3.2. Magnetic Properties. For the calculation of magnetic susceptibilities the formalism given by Ginsberg et al. was used.[2a] Some of the pair wave functions in ref 2a were found to have incorrect phases. For the evaluation of the low-temperature magnetization behavior we proceeded as follows: From the INS it was concluded that the lowest molecular level of the nickel dimer was $|S,M\rangle = |2,\pm 2\rangle$, 6.8 cm^{-1} below $|2,\pm 1\rangle$. The magnetization was then calculated with neglect of all but the lowest $|2,\pm 2\rangle$ level. Account of the higher levels was taken by the inclusion of a second-order Zeeman correction for $H \| x$ and $H \| y$. This is a good approximation for temperatures up to 3.0 K and magnetic fields up to 3 T. Outside this range the full energy matrix has to be diagonalized.

Intermolecular interactions were taken into account by the term[13]

$$\hat{H}' = -2J'\vec{S}\langle\vec{S}\rangle \quad (7)$$

where J' incorporates effects from nearest and more distant neighboring dimers in the lattice, $\vec{S}$ is the dimer spin, and $\langle\vec{S}\rangle$ is its expectation value. Within the above mentioned approximation $\langle S^x\rangle = \langle S^y\rangle = 0$. Considering only $|2,\pm 2\rangle$, we immediately get the following implicit equation for $\langle S^z\rangle$:

$$\langle S^z\rangle = 2\tanh[(-2g^2\mu_B H^z + 4J'\langle S^z\rangle)/kT] \quad (8)$$

Expanding the tanh function in a series and breaking off after the first term, we can approximate $\langle S^z\rangle$:

$$\langle S^z\rangle_{\text{app}} = \frac{-4g^2\mu_B H^z}{kT - 8J'} \quad (9)$$

Equation 9 is a good approximation for small H^z. For the evaluation of energies and Boltzmann factors it is necessary to use eq 8. The first-order magnetic moments of the two levels $|2,\pm 2\rangle$, $\mu^z(+2)$ and $\mu^z(-2)$, respectively, are given by

$$\mu^z(+2) = -\mu^z(-2) = -\frac{\partial E(+2)}{\partial H^z} = -2g^z\mu_B + \frac{8J'}{(\cosh y)^2}\left[-\frac{2g^z\mu_B}{kT} + \frac{4J'}{kT}\left(\frac{-4g^z\mu_B}{kT - 8J'}\right)\right] \quad (10)$$

where $y = (-2g^z\mu_B H^z + 4J'\langle S^z\rangle)/kT$. The second term in the

(12) Furrer, A.; Güdel, H. U. *Phys. Rev. Lett.* **1977**, *39*, 657.

(13) Ginsberg, A. P.; Lines, M. E. *Inorg. Chem.* **1972**, *11*, 2289.

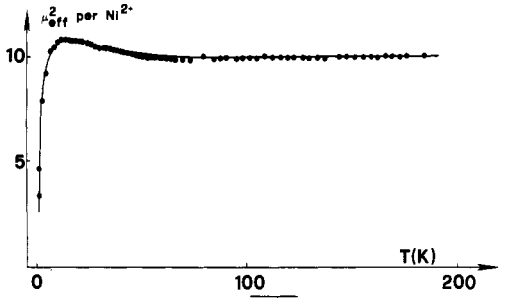

Figure 3. Temperature dependence of μ_{eff}^2. The corresponding values of undeuterated $[Ni_2(en)_4Br_2]Br_2$ are undistinguishable. The full curve corresponds to a calculation with $g_{iso} = 2.25$, $J = 4.0$ cm^{-1}, $D = -6.0$ cm^{-1}, $E = 0.0$ cm^{-1}, and $J' = -0.41$ cm^{-1}.

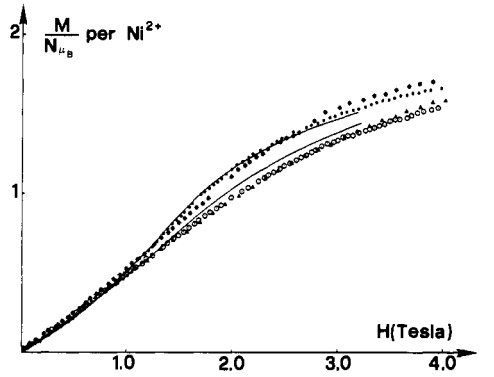

Figure 4. Magnetizations at 1.6 K [(*) deuterated, (●) undeuterated] and 2.7 K [(▲) deuterated, (⊙) undeuterated]. The full curves were calculated with use of the procedure in section 3.2 with $g_{iso} = 2.25$ and $J' = -0.25$ cm^{-1}.

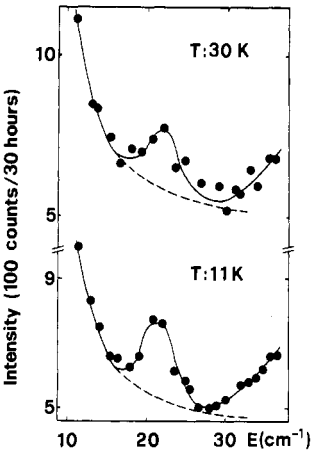

Figure 5. Section of the powder INS spectrum at two temperatures, measured on a MARC spectrometer at the Saphir reactor. The energy of incoming neutrons was 120 cm^{-1}, and resolution (at 100 cm^{-1}) was 5 cm^{-1}. The solid and broken lines are a guide for the eye.

square bracket of (10) was obtained with the approximation (9).

The macroscopic molar magnetic moment M^z is now obtained by summing the magnetic moments μ^z, appropriately weighted by Boltzmann factors:

$$M^z = -2Ng^z\mu_B\left\{1 + \frac{8J'}{(\cosh y)^2 kT}\left[1 + \frac{8J'}{kT - 8J'}\right]\right\}\tanh y \qquad (11)$$

In our approximation $\langle S^x\rangle = \langle S^y\rangle = 0$, and $M^x = M^y$ is simply given by second-order Zeeman perturbation theory as

$$M^x = M^y = -\frac{2N(g^x)^2\mu_B{}^2H^x}{D} \qquad (12)$$

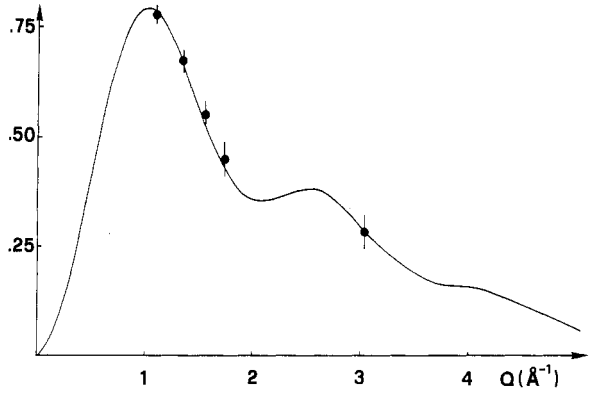

Figure 6. Observed ($T = 11$ K) and calculated (for $\Delta S = \pm 1$, $\Delta M = \pm 1$) Q dependence of the 21-cm^{-1} transition.

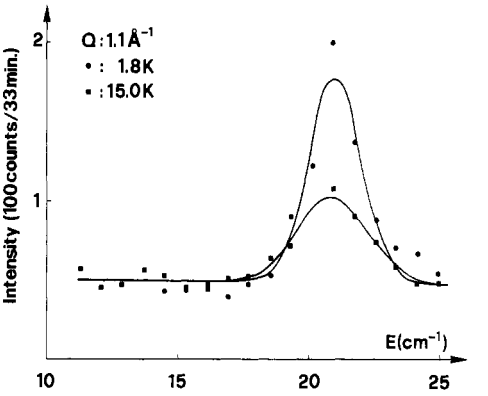

Figure 7. Section of the powder INS spectrum at two temperatures, measured on a triple-axis spectrometer (TAS 7) with use of a cold source at Risø. The energy of the analyzer was fixed at 32 cm^{-1}. Resolution (at 32 cm^{-1}) was 2 cm^{-1}. The full curves represent least-squares fits to the data approximating the peaks by Gaussians.

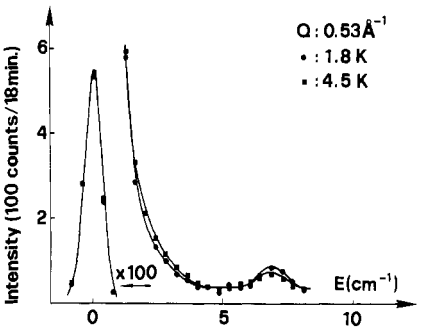

Figure 8. As for Figure 7, but for two different temperatures and a different range of energy transfer. A beryllium filter was used. The energy of the analyzer was fixed at 32 cm^{-1}. Resolution (at 32 cm^{-1}): 0.9 cm^{-1}.

Due to the implicit nature of eq 8, $\langle S^z\rangle$ was computed self-consistently.

4. Results

Figure 3 shows the powder magnetic susceptibility of $[Ni_2(en)_4Br_2]Br_2$ between 190 and 1.6 K. Observed magnetization curves at 1.6 and 2.7 K are displayed in Figure 4. A survey INS powder spectrum, measured at Würenlingen, is given for two temperatures in Figure 5. The width of the peak around 21 cm^{-1} is determined by the instrumental resolution. The peak can be identified as magnetic scattering from its Q dependence, which is given in Figure 6, together with the calculated Q dependence for a $\Delta S = \pm 1$, $\Delta M = \pm 1$ transition. Scattering caused by phonons increases with increasing Q, and the temperature dependence is determined by Bose statistics.

Table II. Nonvanishing Matrix Elements $\langle SM|\hat{S}_i^{\alpha}|S'M'\rangle$[a]

S	M	S'	M'	$\langle SM\|\hat{S}_a^z\|S'M'\rangle$	S	M	S'	M'	$\langle SM\|\hat{S}_a^x\|S'M'\rangle$	$\langle SM\|\hat{S}_a^y\|S'M'\rangle$
0	0	1	0	0.816	0	0	1	−1	0.577	−0.577*i*
1	0	2	0	0.577	0	0	1	1	−0.577	−0.577*i*
1	1	1	1	0.50	1	0	1	−1	0.354	−0.354*i*
1	−1	1	−1	−0.50	1	0	1	1	0.354	0.354*i*
1	1	2	1	0.50	1	0	2	−1	0.354	−0.354*i*
1	−1	2	−1	0.50	1	0	2	1	−0.354	−0.354*i*
2	1	2	1	0.50	1	−1	2	−2	0.50	−0.50*i*
2	−1	2	−1	−0.50	1	−1	2	0	−0.204	−0.204*i*
2	2	2	2	1.00	1	1	2	0	0.204	−0.204*i*
2	−2	2	−2	−1.00	1	1	2	2	−0.50	−0.50*i*
					2	0	2	−1	0.612	−0.612*i*
					2	0	2	1	0.612	0.612*i*
					2	−1	2	−2	0.50	−0.50*i*
					2	1	2	2	0.50	0.50*i*

[a] Elements not listed are obtained by the following relations:

$$\langle SM|\hat{S}_b^{\alpha}|S'M'\rangle = (-1)^{S-S'}\langle SM|\hat{S}_a^{\alpha}|S'M'\rangle$$
$$\langle SM|\hat{S}_i^{\alpha}|S'M'\rangle = \langle S'M'|\hat{S}_i^{\alpha}|SM\rangle \text{ for } \alpha = x, z$$
$$\langle SM|\hat{S}_i^{\alpha}|S'M'\rangle = -\langle S'M'|\hat{S}_i^{\alpha}|SM\rangle \text{ for } \alpha = y$$

On both grounds phonon scattering is ruled out as an origin of the 21-cm^{-1} peak. Figures 7 and 8 show triple-axis powder INS spectra, measured at Risø with use of a cold source. Due to the higher resolution (0.9 cm^{-1} as compared to 5 cm^{-1} in Figure 5) a new well-defined peak appears at 6.8 cm^{-1}. Again it can easily be identified as magnetic from its Q dependence. From the Q dependence it can further be concluded that the corresponding transitions must have $\Delta S = 0$. The spectrum at $T = 1.8$ K and $Q = 1.0$ Å^{-1} was measured up to an energy transfer of 40 cm^{-1}. No additional peaks were found. Figures 9 and 10 contain the results of a set of single-crystal INS experiments.

5. Analysis and Discussion

As the dimeric $[Ni_2(en)_4Br_2]^{2+}$ units (Figure 1) are shielded by the rather bulky en ligands and well separated from one another, the magnetic properties must be dominated by intramolecular effects at all but the very lowest temperatures. The shape of the μ_{eff}^2 curve (Figure 3) between 70 and 15 K is typical of ferromagnetic intramolecular coupling. Zero-field splittings and possibly a small antiferromagnetic intermolecular interaction cause the sharp drop between 15 and 1.6 K.[2a] There is no indication of a transition to an ordered magnetic phase down to 1.6 K. The sigmoidal behavior of the 1.6 K magnetization (Figure 4) with an inflection point between 1 and 1.5 T can be explained by intramolecular or short-range intermolecular effects. If the origin was intramolecular, the effect could be brought about by an axial zero-field splitting with positive D (right-hand side of Figure 2). In this picture the inflection point of the magnetization would correspond to a spin-crossover point. There are nice examples of such situations in the literature.[14] The low-temperature magnetization behavior could, on the other hand, have its origin in small intermolecular interactions. A convincing discrimination between the two possibilities is possible from the analysis of the INS data.

All the magnetic scattering intensity is concentrated in the two peaks at 6.8 and 21 cm^{-1}. Both of them show a slight increase of intensity on lowering the temperature from 4.5 to 1.8 K. They differ markedly in their $\vec{Q}$ dependence. To a good approximation, the 6.8-cm^{-1} peak shows the behavior expected for $\Delta S = 0$ transitions. The $\vec{Q}$ dependence of the 21-cm^{-1} peak is in qualitative agreement with theoretical expectations for $\Delta S = \pm 1$ transitions; quantitatively there are considerable

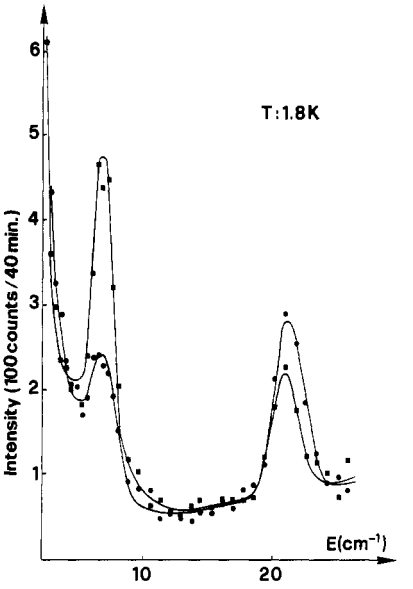

Figure 9. Result of single-crystal INS experiments: $\vec{Q}\cdot\vec{R} = 0.28, 1 - (Q_z^2/Q^2) = 0.17$ (■); $\vec{Q}\cdot\vec{R} = 2.13, 1 - (Q_z^2/Q^2) = 0.83$ (●). The analyzer energy was 32 cm^{-1}, and the resolution (at 32 cm^{-1}) was 1.6 cm^{-1}. The full curves are Gaussian fits to the peaks.

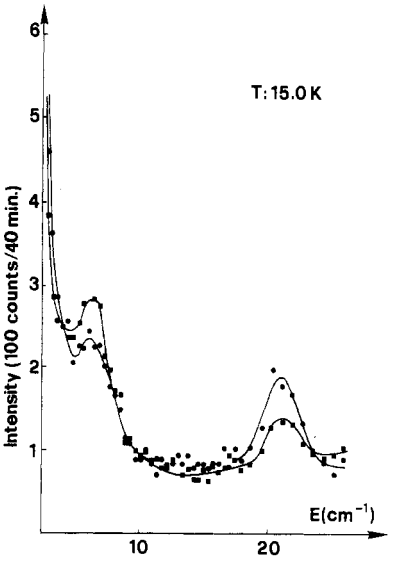

Figure 10. As for Figure 9, but for $T = 15$ K.

(14) Carlin, R. L.; van Duyneveldt, A. J. *Acc. Chem. Res.* **1980**, *13*, 231.

Table III. Observed and Calculated Inelastic Neutron Scattering Transition Energies and Intensities

Single-Crystal Experiment

peak	T, K	$\vec{Q}$, Å^{-1}	$\vec{Q}\cdot\vec{R}$	$1-(Q_z^2/Q^2)$	main transition	E_{obsd}, cm^{-1}	E_{calcd}, cm^{-1}	I_{obsd}	I_{calcd}
A	1.7	1.05	0.28	0.17	$\|2,\pm2\rangle \rightarrow \|2,\pm1\rangle$	6.91 ± 0.05	6.8	1.00 ± 0.08[a]	1.00[a]
A	15.0	1.05	0.28	0.17		6.48 ± 0.09		0.47 ± 0.08	0.49
A	1.7	1.05	2.13	0.83		6.94 ± 0.11		0.27 ± 0.13	0.15
A	1.7	1.05	2.48	0.96		6.80 ± 0.30		0.16 ± 0.13	0.06
A	1.7	0.50	0.00	0.11		6.85 ± 0.10		1.25 ± 0.10	1.15
A	1.7	2.00	0.00	0.11		6.70 ± 0.20		0.67 ± 0.10	0.79
B	1.7	1.05	2.13	0.83	$\|2,\pm2\rangle \rightarrow \|1,\pm1\rangle$	21.04 ± 0.11	21.0	0.79 ± 0.10	0.50
B	15.0	1.05	2.13	0.8		20.90 ± 0.10		0.51 ± 0.10	0.25
B	1.7	1.05	0.28	0.17		20.92 ± 0.10		0.47 ± 0.10	0.02
B	15.0	1.05	0.28	0.17		21.01 ± 0.2		0.22 ± 0.10	<0.01
B	1.7	2.75	5.52	0.83		20.95 ± 0.3		0.40 ± 0.10	0.05
C	15.0	1.05	2.13	0.83	$\|2,\pm1\rangle \rightarrow \|1,\pm1\rangle$	(~14.2)	14.2	0.00 ± 0.10	0.09

Powder Experiment

peak	T, K	$\vec{Q}$, Å^{-1}	main transition	E_{obsd}, cm^{-1}	E_{calcd}, cm^{-1}	I_{obsd}	I_{calcd}
A	1.8	0.20	$\|2,\pm2\rangle \rightarrow \|2,\pm1\rangle$	6.7 ± 0.5	6.8	1.00 ± 0.10[a]	1.00[a]
A	4.5	0.20		6.6 ± 0.5		0.80 ± 0.10	0.85
A	1.8	0.525		6.94 ± 0.08		0.68 ± 0.10	0.68
A	4.5	0.525		6.82 ± 0.06		0.53 ± 0.10	0.60
B	11.0	1.10	$\|2,\pm2\rangle \rightarrow \|1,\pm1\rangle$	21.75 ± 0.05	21.0	1.14 ± 0.10	1.16
B	11.0	1.34		21.2 ± 0.5		1.00 ± 0.10[a]	1.00[a]
B	11.0	1.56		21.2 ± 0.5		0.83 ± 0.10	0.79
B	11.0	1.76		21.75 ± 0.5		0.68 ± 0.10	0.63
B	11.0	3.00		21.2 ± 0.5		0.44 ± 0.10	0.42
B	11.0	1.17		21.0 ± 0.5		1.00 ± 0.10[a]	1.00[a]
B	30.0	1.17		21.3 ± 0.5		0.72 ± 0.15	0.64
B	1.8	1.10	$\|2,\pm2\rangle \rightarrow \|1,\pm1\rangle$	21.0 ± 0.1	21.0	1.00 ± 0.08[a]	1.00[a]
B	4.5	1.10		21.0 ± 0.3		0.80 ± 0.10	0.87
B	15.0	1.10		20.9 ± 0.1		0.56 ± 0.08	0.51
B	1.8	1.50		21.2 ± 0.5		0.80 ± 0.10	0.75
B	1.8	2.0		21.0 ± 0.5		0.46 ± 0.10	0.48
A	15.0	1.10	$\|2,\pm2\rangle \rightarrow \|2,\pm1\rangle$	6.6 ± 0.5	6.8	0.54 ± 0.10	0.53
C	15.0	1.10	$\|2,\pm1\rangle \rightarrow \|1,\pm1\rangle$	(~14.2)	14.2	0.00 ± 0.10	0.08

[a] Normalized to 1.

Table IV. Final Parameters (cm^{-1})

$J = 3.55 \pm 0.20$	$E = 0.0 \pm 0.8$
$D = -6.8 \pm 0.8$	$J' = -0.25 \pm 0.05$

deviations. The reasons for these will be discussed below.

Table II gives the relevant matrix elements of INS intensity for all the allowed transitions. There are many possible transitions with comparable contributions to the scattering cross section. The observation of only two peaks therefore means that each is composed of more than one transition. There is only one physically reasonable splitting pattern compatible with that; it is shown in Figure 11. Arrows indicate the allowed transitions contributing to the observed peaks. Quantitative agreement between observed and calculated intensities and their temperature dependencies is necessary to confirm the picture in Figure 11. This is shown in Table III. The allowed "hot" transition $|2,\pm1\rangle \rightarrow |1,\pm1\rangle$ has a very low intensity, in agreement with the 15 K experiment. The splitting pattern of Figure 11 can be reproduced by a Hamiltonian (1b) with the parameters $J = 3.55 \pm 0.20$ cm^{-1} and $D = -6.8 \pm 0.8$ cm^{-1}. The simplicity and regularity of the splitting, which lead to the coincidences of INS transitions, are caused by the equality between $-2J$ and D. There is no need to introduce a rhombic term in the Hamiltonian. The width of the 6.8-cm^{-1} INS peak at half-height, 1.6 cm^{-1}, is the same as that of the elastic peak. It is determined by the instrumental resolution. As $|2,\pm2\rangle$ is split only in second order by a rhombic crystal field term, 1.6 cm^{-1} is an upper limit for the possible first-order splitting of $|2,\pm1\rangle$ and therefore $|E| < 0.8$ cm^{-1}.

Having thus established the intramolecular splitting pattern we consider intermolecular effects in detail. The absence of any long-range order above 1.6 K is confirmed by the absence of a dispersion of transition energies in the 1.8 K INS results. This agrees with similar findings in copper(II) acetate,[15] and

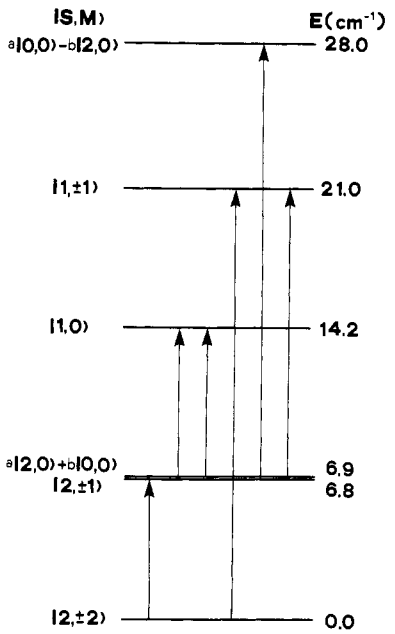

Figure 11. Final result of the INS analysis. The intramolecular splitting is due to ferromagnetic exchange coupling and axial magnetic anisotropy. Parameters: $J = 3.55 \pm 0.20$ cm^{-1}, $D = -6.8 \pm 0.8$ cm^{-1}, $a = 0.947$ and $b = 0.321$.

(15) Güdel, H. U.; Stebler, A.; Furrer, A. *J. Phys. C* **1980**, *13*, 3817.

it confirms the molecular localized nature of the magnetic excitations.

The differences between observed and theoretical $\vec{Q}$ dependencies (vide supra) may have three principal physical origins: (i) underlying phonon scattering, (ii) multiple scattering, and (iii) intermolecular interactions. We cannot rule out a contribution from (i). The high concentration of hydrogen atoms in the sample (8 H per 1 Ni) is mainly responsible for multiple scattering. Due to the extremely high incoherent nuclear scattering amplitude of hydrogen, a large portion of the incoming neutrons are scattered incoherently by hydrogen atoms before they reach a magnetic center. As a result the neutrons interacting with the magnetic centers do not all have the same wave vector, $\vec{Q}$ is no longer well defined, and relation 4 becomes soft. A quantitative estimate of these effects is difficult. We feel that it accounts for at least part of the observed discrepancies.

Deviations from theoretical Q dependencies may also arise through intermolecular interactions (short-range order). If, instead of one nickel dimer, we consider a pair of dimers with weak interaction between them, there will be some INS intensity depending on cos $(\vec{Q}\cdot\vec{R}_{id})$, where $\vec{R}_{id}$ is the shortest interdimer Ni–Ni vector. The relative magnitude of that intensity should, however, be small.

Returning to the magnetic properties, we can now interpret the inflection of the low-temperature magnetization as a result of intermolecular interactions, since the intramolecular splitting pattern corresponds to the left-hand side of Figure 2. Using the molecular field approach described in section 3, i.e., assuming the molecular field to be induced by the magnetization resulting from the external magnetic field, we can calculate magnetization curves for various values of J'.

Sigmoidal curves are obtained for $T < 2.5$ K and J' around -0.25 cm^{-1}, and they give a good reproduction of the experimental data (Figure 4). A literature value of $g = 2.25$ (isotropic) was used, and no attempt was made to get the best fit to the data by varying both J' and g. The observed differences of low-temperature magnetizations between N-deuterated and undeuterated $[Ni_2(en)_4Br_2]Br_2$ are very small. Due to the strong temperature dependence of the effects they may have an experimental and not a physical origin.

For comparison purposes we attempted to determine the relevant parameters from the temperature dependence of the magnetic susceptibility. As it is impossible to extract five parameters from the data in Figure 3, we fixed $g = 2.25$ (literature) and $E = 0$ (from INS). The following values were then obtained from the least-squares fit: $J = 4.0$ cm^{-1}, $D = -6.0$ cm^{-1}, $J' = -0.4$ cm^{-1}. The agreement with the INS values is reasonable. It is undoubtedly somewhat fortuitious (cf. Table I) because the "correct" values were used as starting parameters and also partial use of the INS results ($E = 0$) was made.

The low-temperature magnetization measurements (Figure 4) are a much more sensitive probe of the intermolecular interactions than is the magnetic susceptibility. Therefore, the J' value determined from the magnetizations is more trustworthy. A comparison of the parameters determined in this study with those of related systems shows J to be well within the range of exchange parameters reported for di-μ-bromo and di-μ-chloro bridged species.[4,2,16] The ferromagnetic sign can be rationalized in terms of Kanamori–Goodenough rules or more sophisticated theoretical models. $|D|$ values reported for mononuclear nickel(II) complexes range from 0 to 6 cm^{-1}.[17] Values of up to 22 cm^{-1} have been proposed on the basis of heat capacity and magnetic susceptibility measurements for the linear chain compounds NiX_2L_2 (X = Cl, Br; L = pyridine, pyrazole).[2b] Both sign and magnitude of J' appear reasonable.

Acknowledgment. We are indebted to K. Mattenberger and O. Vogt for the magnetization and susceptibility measurements. This work was supported by the Swiss National Science Foundation (Grant No. 2.869-0.77). We thank the Berner Hochschulstiftung for a travel grant.

(16) Lines, M. E. *Phys. Rev.* **1963**, *131*, 546.
(17) Landolt-Börnstein, "Physikalische und Chemische Tabellen"; Springer-Verlag: Berlin, 1966; Neue Serie II/2, pp 4–57. *Ibid.*, 1976; Neue Serie II/8, p 1059.

Contribution from the Chemical Physics Group, Tata Institute of Fundamental Research, Colaba, Bombay 400 0005, India

Proton Magnetic Resonance Studies on High-Spin Iron(III) Porphyrins

D. V. BEHERE, R. BIRDY, and S. MITRA*

Received July 22, 1981

Results of isotropic proton magnetic resonance studies on a series of high-spin five-coordinated (tetraphenylporphinato)iron(III) complexes, Fe(TPP)X (X = NCS, Cl, Br, I), have been reported. Measurements have been done at 270 MHz in $CDCl_3$ solution between 238 and 328 K. The temperature-dependent isotropic shifts show increasing deviation from $1/T$ dependence from X = NCS to I. Further, the isotropic shifts for the phenyl protons show certain anomalies in sign and magnitude. These observations have been rationalized in terms of large dipolar shifts, which have been very accurately determined in the present work by using our experimental values of single-crystal susceptibility data. The dipolar-shift contribution is, as expected, quite large for the phenyl protons but is also significant for the pyrrole protons, being about 18% of the total shift for Fe(TPP)Br at 238 K. The contact shift for the phenyl protons, though much smaller in magnitude than that of the pyrrole protons, is however not insignificant and constitutes about half of the total shift. An analysis of the isotropic shift data using the theory of Kurland and McGarvey gives accurate values for the hyperfine coupling constants of these high-spin molecules and suggests that the zero-field splitting of the $^6A_1$ ground state is nearly the same in the solid as in the chloroform solution.

Introduction

Proton magnetic resonance studies on synthetic iron(III) porphyrins have been very useful in understanding and assigning the more complex NMR spectra of heme proteins.[1-3] These studies have also helped in understanding the nature of the metal–ligand bonding and the distribution of unpaired-electron spin density across the porphyrin skeleton.[4-6]

(1) La Mar, G. N.; Walker, F. A. In "The Porphyrins"; Dolphin, D., Ed.; Academic Press: New York, 1978; Vol. IVB, p 61.
(2) Walker, F. A.; La Mar, G. N. *Ann. N.Y. Acad. Sci.* **1973**, *206*, 328.
(3) (a) La Mar, G. N., Horrocks, W. D., Holm, R. H., Eds. "NMR of Paramagnetic Molecules"; Academic Press: New York, 1973. (b) La Mar, G. N. In ref 3a.

0020-1669/82/1321-0386$01.25/0